REGULAR ARTICLE

The low-lying electronic states of BeAs: a first principles characterization

Tiago Vinicius Alves · Willian Hermoso · Fernando R. Ornellas

Abstract The electronic structure and spectroscopic properties of a manifold of states of a new molecular species, BeAs, have been investigated theoretically at the complete active space self-consistent field/multireference single and double excitations configuration interaction (CASSCF/MRSDCI) approach, using the aug-cc-pV5Z-PP basis set for arsenic, which includes a relativistic effective core potential, and the cc-pV5Z set for beryllium. Potential energy curves of five quartet and eight doublet $(\Lambda + S)$ states correlating with the five lowest-lying dissociation limit are constructed. The effect of spin–orbit coupling is also included in the description of the ground state, and of the doublet states correlating with the second dissociation channel. Dipole moment functions and vibrationally averaged dipole moments are also evaluated. The similarities and differences between BeAs, BeP, and BeN are analyzed. Spin–orbit effects are small for the ground state close to the equilibrium distance, but avoided crossings between $\Omega = 1/2$ states, and between $\Omega = 3/2$ states changes significantly the $\Lambda + S$ curves for the lowest-lying doublets.

Keywords Beryllium arsenide ·
CASSCF/MRCI calculations · Potential energy curves ·
Spectroscopic properties · Spin–orbit effects

T. V. Alves · W. Hermoso · F. R. Ornellas (✉)
Departamento de Química Fundamental, Instituto de Química,
Universidade de São Paulo, Caixa Postal 26077,
São Paulo, SP 05513-970, Brazil
e-mail: frornell@usp.br

1 Introduction

Over the years, our group has spent considerable effort in describing the properties of a variety of new molecular species, and in providing reliable spectroscopic information of a manifold of electronic states of other molecules for which very little was known. Beryllium-containing diatomics, in particular, have been the focus of several investigations involving neutral species like BeH [1], BeB [2], BeC [3], BeN [4], BeF [5], and BeP [6], as well as ionic ones such as BeH$^+$ [7], BeC$^+$ [8], and BeF$^+$ [9]. For all these molecules, our goal was to characterize as detailed and as accurately as possible all the electronic states correlating with the lowest-lying dissociation channels, thus providing reliable spectroscopic data that could motivate and guide spectroscopists in the experimental investigation of these species. Considering the hazards associated with the manipulation of beryllium-containing compounds, which are known to be carcinogenics, their spectra characterization is a valuable source of reference data.

Following the same line of theoretical work carried out for the above diatomics, our focus of investigation in this study is a new beryllium species, namely BeAs, now involving the element arsenic, well known as an active poison. Here, our major goal is also to provide a very reliable and accurate spectroscopic characterization of a manifold of electronic states correlating with the lowest-lying dissociation channels; this description includes potential energy curves, vibrational states, spectroscopic constants, dipole moment functions, and spin–orbit corrections to a set of low-lying states. Since, to the best of our knowledge, neither experimental nor theoretical studies have been yet found in the literature on this system, it is our hope that the data here reported can also motivate and further guide its experimental investigation.

2 Methodology

The methodological approach used follows essentially that employed for the investigation of its isovalent partners BeN and BeP. First, with the use of the Wigner–Witmer rules [10], the possible electronic states correlating with the five lowest-lying dissociation channels of the molecule were identified; as shown in Table 1, there are at all 12 quartets, 16 doublets, and 2 sextets. In this work, however, we focused mainly on the description of all quartet and doublet states correlating with the four lowest-lying dissociation channels only. The sextets are expected to be repulsive and to lie very high in energy. For the quartets, they correspond to a $^4\Sigma^-$ correlating with the first channel, a $^4\Pi$ and another $^4\Sigma^-$ correlating with the fourth channel; since test calculations indicated the presence of another relatively low-lying $^4\Pi$ state, it was also included in the overall description. This extra state dissociates into the fifth channel. Additionally, attempts were also made to locate another bound state of A_1 symmetry (C_{2v} point group), which could correspond to either a $^4\Sigma^+$ or a $^4\Delta$ symmetry in the $C_{\infty v}$ point group; test calculations, however, revealed it to be a $^4\Sigma^+$. For the doublets, our investigation includes eight states, the first three ($^2\Sigma^-$, $^2\Pi$, and $^2\Delta$) associated with the second channel, two states ($^2\Sigma^+$ and $^2\Pi$) correlating with the third channel, another two ($^2\Sigma^-$ and $^2\Pi$) dissociating into the fourth channel, and a last one ($^2\Pi$) with the fifth channel. In the case of doublets, we essentially accounted for all states correlating with the first four channels and another $^2\Pi$ state dissociating into the fifth channel; this extra state was also included to better describe the regions where avoided crossings were found in previous investigations in our group concerning the isovalent species BeN and BeP.

The electronic wavefunctions describing these states have built in both static or near degeneracy correlations effects through the complete active space self-consistent field (CASSCF) approach [11, 12], and dynamical correlation effects via the multireference singles and doubles configuration interaction (MRSDCI) method [13, 14], thus guaranteeing a reliable and accurate characterization of the electronic structure of a manifold of states until the dissociation limit, as extensively verified in previous studies in the literature. All calculations were done in the C_{2v} point group symmetry, a restriction inherent in the computational codes. To construct the zero-order wavefunction, allowance was made for all possible distributions of 9 electrons in an active space consisting of the 12 orbitals (6, 3, 3, 0); besides the valence orbitals, this set also contained an extra set of three correlating orbitals, one of A_1 symmetry, and one of each of the B_1 and B_2 symmetries. A common set of molecular orbitals were next obtained by optimizing an average energy comprising the states (shown in parentheses) of each symmetry, $A_1(4)$, $B_1(2)$, $B_2(2)$, $A_2(4)$, with equal weights for the quartets states, and $A_1(3)$, $B_1(4)$, $B_2(4)$, $A_2(3)$ for the doublets. Next, for each one of the spin symmetries, the diagonalization of the state-averaged density matrix generated a common set of natural orbitals that were employed in the subsequent MRSDCI step. The dimensions of the configuration state functions (CSFs) generated were 37,536 for the A_1 (Σ^+, Δ) symmetry, 37,752 for B_1 (Π), and 37,968 for A_2 (Σ^-, Δ), for the quartets, and 47,676 for the A_1 (Σ^+, Δ) symmetry, 47,190 for B_1 (Π), and 46,704 for A_2 (Σ^-, Δ), for the doublets. Since the generation of all single and double excitations from reference spaces with the above dimensions is computationally very demanding, new reduced reference spaces were constructed by selecting all CSFs with coefficients greater than 0.015 in absolute magnitude from the CASSCF wavefunctions. Then dynamical correlation effects were next incorporated by allowing all single and double excitations on top of these reduced reference spaces. A further reduction in the dimensions of the final wavefunctions was accomplished by the internally contracted multireference configuration interaction (iCMRCI) approach [13, 14], as implemented in the Molpro-2006

Table 1 Low-lying (Λ + S) electronic states of the molecule BeAs, their dissociation channels, and energy at the dissociation limit

State of separated atoms	Molecular states	ΔE (cm^{-1})	
		Theor.[a]	Exp.
Be (^1S_g) + As (^4S_u)	$^4\Sigma^-$	0.0	0.0
Be (^1S_g) + As (^2D_u)	$^2\Sigma^-$, $^2\Pi$, $^2\Delta$	10,634	10,786.0[b]
Be (^1S_g) + As (^2P_u)	$^2\Sigma^+$, $^2\Pi$	18,158	18,493.9[c]
Be (^3P_u) + As (^4S_u)	$^{2,4,6}\Sigma^-$, $^{2,4,6}\Pi$	22,166	21,980.2[d]
Be (^3P_u) + As (^2D_u)	$^{2,4}\Sigma^+$, $^{2,4}\Sigma^-$ (2), $^{2,4}\Pi$ (3), $^{2,4}\Delta$ (2), $^{2,4}\Phi$	32,998	32,766.2

[a] Calculated at $R = 50.0$ a_0, CASSCF/MRSDCI. Basis sets: Be(cc-pV5Z), As(aug-cc-pV5Z-PP)

[b] Weighted average over the atomic multiplets 10,592.7 ($^2D_{3/2}$) and 10,914.9 ($^2D_{5/2}$) of As; Ref. [25]

[c] Weighted average over the atomic multiplets 18,186.3 ($^2P_{1/2}$) and 18,647.7 ($^2P_{3/2}$) of As; Ref. [25]

[d] Weighted average over the atomic multiplets 21,978.3 ($^3P_0$), 21,978.9 ($^3P_1$), and 21,981.3 ($^3P_2$), of As; Ref. [25]

suite of programs [15], thus leading to expansions of the order of 3×10^6 to 5×10^6 terms depending on the state symmetry and also on the internuclear distance.

The atomic functions used in the construction of the molecular orbitals were the correlation consistent polarized valence quintuple-zeta set (cc-pV5Z) for beryllium (http://www.emsl.pnl.gov/forms/basisform.html), and the aug-cc-pV5Z-PP set developed by Peterson et al. [16] for arsenic. The arsenic set included a small core (10 electrons) energy consistent relativistic pseudo-potential (PP), namely, ECP10MDF, that is, the $1s$-$2p$ core was replaced by an energy consistent pseudo-potential that was optimized in a multiconfigurational Dirac–Hartree–Fock calculation. Vibrational energies and wavefunctions were computed as solutions of the radial Schrödinger equation for the nuclear motion using the Numerov–Cooley method as implemented in the INTENSITY program [17]. The potential energy functions were generated by numerical interpolation of the total energies (electronic plus nuclear repulsion) calculated at about 60 internuclear distances; these energies include the Davidson estimate to the full configuration interaction limit (MRCI + Q) [18, 19]. As detailed in previous works of our group [20–23], spectroscopic constants were obtained by standard fitting procedures.

The contribution of spin–orbit effects was assessed only for the group of doublet states ($^2\Pi$, $^2\Delta$, and $^2\Sigma^-$) dissociating into the second channel and the ground state curve (X $^4\Sigma^-$), which is the only state correlating with the first dissociation channel. The calculations were done at the CASSCF/MRSDCI level using the state interacting approach [24] whereby the spin–orbit eigenstates are obtained by the diagonalization of a matrix of the electronic and spin–orbit operators (H_{el} + H_{SO}) in a basis of (Λ + S) eigenstates of H_{el}. The active space was reduced to (5, 2, 2, 0) functions, and a triple-zeta basis set of the same type as those described above was employed. It is worth noting that the spin–orbit parameters that accompany the pseudopotential were used in all cases.

3 Results and discussion

3.1 Potential energy curves and states composition

In Figs. 1 and 2, energy profiles are presented depicting the potential energy curves (PECs) of eight doublet and five quartet (Λ + S) states, respectively, ranging from the equilibrium until the dissociation regions; the associated equilibrium internuclear distances, the adiabatic excitation energies, and a collection of vibrational and rotational spectroscopic constants are collected in Table 2. Numerical
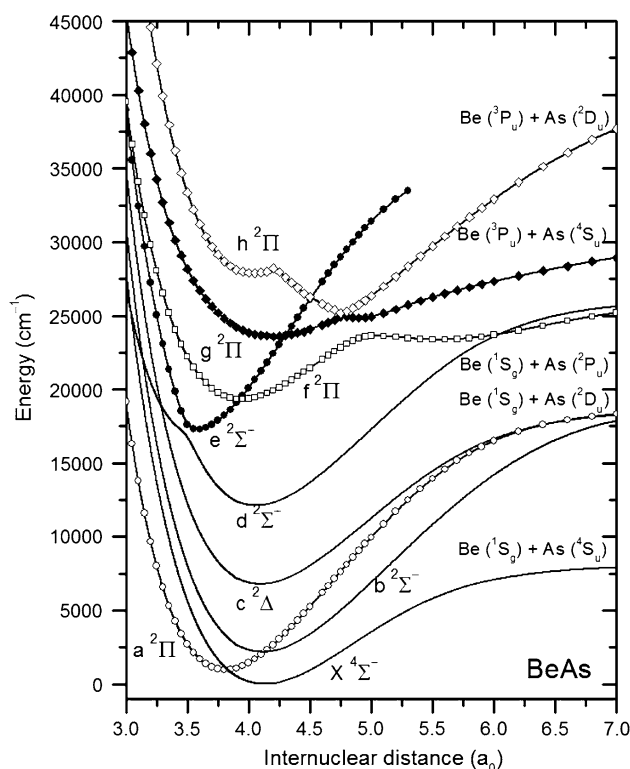

Fig. 1 Potential energy curves for the ground state, X $^4\Sigma^-$, and the lowest-lying doublet states of the molecule BeAs
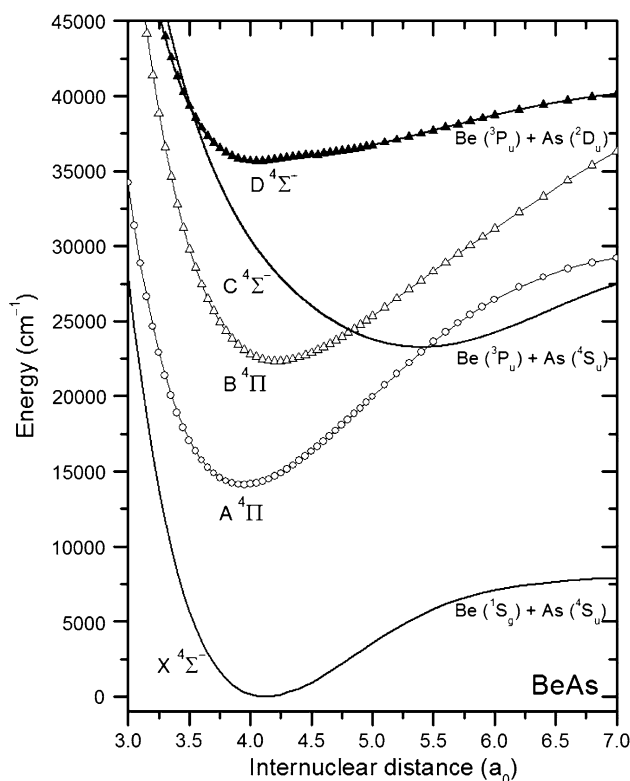

Fig. 2 Potential energy curves for the lowest-lying quartet states of the molecule BeAs

Table 2 Adiabatic excitation energies (in cm^{-1}), equilibrium distance (in a_0), rotational and vibrational constants (in cm^{-1}), and dissociation energies (in kcal/mol) for the BeAs species

	T_e	R_e	B_e	ω_e	$\omega_e x_e$	$\omega_e y_e$	D_e
$X\ ^4\Sigma^-$	0	4.133	0.4385 (9)	500.8 (15)	1.508	−0.213	23.87
$a\ ^2\Pi$	933	3.812	0.5152 (9)	674.2 (18)	5.709	0.072	51.95
$b\ ^2\Sigma^-$	2,107	4.108	0.4438 (7)	585.8 (7)	7.742	0.231	48.48
$c\ ^2\Delta$	6,802	4.114	0.4426 (9)	527.4 (10)	0.258	−0.146	34.54
$d\ ^2\Sigma^+$	12,093	4.059	0.4544 (4)	566.1 (4)	2.543	−0.051	40.92
$A\ ^4\Pi$	14,111	3.959	0.4767 (9)	553.8 (15)	2.550	−0.003	46.64
$e\ ^2\Sigma^+$	17,172	3.604	0.5765 (6)	1,150.7 (5)	63.294	4.375	46.60
$f\ ^2\Pi$	19,321	3.936	0.4842 (5)	555.2 (5)	2.421	−0.405	20.25
$B\ ^4\Pi$	22,335	4.195	0.4250 (7)	504.8 (14)	5.245	0.070	53.43
$C\ ^4\Sigma^-$	23,242	5.397	0.2566 (6)	301.2 (5)	1.038	−0.002	20.50
$g\ ^2\Pi$	23,574	4.197	0.4259 (3)	400.7 (2)	−16.420	–	19.57
$h\ ^2\Pi$	25,298	4.755	0.3308 (3)	764.7 (3)	46.453	3.015	45.58
$D\ ^4\Sigma^+$	35,678	4.050	0.4449 (8)	346.6 (8)	13.814	0.587	15.92

Numbers in parentheses refer to the number of points used in the numerical fitting

values of the energies are available upon request to the authors.

The overall picture of the PECs is very similar to that of BeN and of BeP. The ground state is also of $^4\Sigma^-$ symmetry and, at the equilibrium distance (4.133 a_0), it can be characterized by the electronic configuration $1\sigma^2\ 2\sigma^2\ 3\sigma^2$ $1\pi^4\ 4\sigma^2\ 5\sigma^2\ 6\sigma^2\ 1\delta^4\ 2\pi^4\ 3\pi^4\ 7\sigma^2\ 8\sigma^2\ 9\sigma^2\ 4\pi^2\ 10\sigma^1$ ($c_0 \approx 0.93$). As noted above, the inner core of ten electrons is associated with the inner core of the arsenic atom, which was represented by pseudo-potential. The next quartet, $A\ ^4\Pi$ ($R_e = 3.959\ a_0$), with an adiabatic excitation energy of 14,111 cm^{-1}, can be symbolized by the configuration $\ldots 7\sigma^2\ 8\sigma^2\ 9\sigma^1\ 4\pi^3\ 10\sigma^1$ ($c_0 \approx 0.91$), which can be viewed as resulting from the $9\sigma \to 4\pi$ electronic promotion. In this study, a second $B\ ^4\Pi$ state ($R_e = 4.195\ a_0$, $T_e = 22,335$ cm^{-1}), not described in our previous studies of BeN and BeP, is best accounted for by the $\ldots 7\sigma^2\ 8\sigma^2$ $9\sigma^2\ 4\pi^2\ 5\pi^1$ ($c_0 \approx 0.87$) electronic configuration. At about the same energy, we located the state $C\ ^4\Sigma^-$ ($T_e = 23,242$ cm^{-1}) with a relatively large internuclear distance (5.397 a_0); this state is best described as a mixture of configurations $\ldots 7\sigma^2\ 8\sigma^2\ 9\sigma^1\ 4\pi^2\ 10\sigma^2$ ($c_0 \approx 0.77$) and $\ldots 7\sigma^2\ 8\sigma^2\ 9\sigma^2\ 4\pi^2\ 11\sigma^1$ ($c_0 \approx 0.39$). Finally, a much higher $D\ ^4\Sigma^+$ state ($R_e = 4.050\ a_0$; $T_e = 35,678$ cm^{-1}) completes the quartets characterization; this state can be associated with the configuration $\ldots 7\sigma^2\ 8\sigma^2\ 9\sigma^1\ 4\pi^3\ 5\pi^1$ ($c_0 \approx 0.65$). We note that the $B\ ^4\Pi$ and $D\ ^4\Sigma^+$ states become practically degenerate at about 10 a_0. As to the nature of the orbitals associated with these configurations, the $4\pi_{x(y)}$ orbital can be basically described as a bonding combination of the $2p_{x(y)}$ and $4p_{x(y)}$ atomic orbitals of Be and As, respectively, and highly polarized toward the As atom; with an increase in the internuclear distance, this orbital transforms into the As $4p$ orbital. On the other hand, the 10σ orbital, which becomes the As $4p_z$ orbital in the dissociation limit, at the equilibrium distance is basically a

Be polarized antibonding combination of an sp hybrid on Be with an sp hybrid on As. The 8σ and 9σ orbitals also involve bonding and antibonding combinations of sp hybrids, respectively, and at the dissociation limit, they correlate with the As $4s$ and Be $2s$ orbitals.

In the case of the doublets, at the equilibrium distance, the states $b\ ^2\Sigma^-$ ($R_e = 4.108\ a_0$, $T_e = 2,107$ cm^{-1}), $c\ ^2\Delta$ ($R_e = 4.114\ a_0$, $T_e = 6,802$ cm^{-1}), and $d\ ^2\Sigma^+$ ($R_e = 4.059$ a_0, $T_e = 12,093$ cm^{-1}) can be represented by the same electronic configuration as that of the ground state $X\ ^4\Sigma^-$, namely, $\ldots 7\sigma^2\ 8\sigma^2\ 9\sigma^2\ 4\pi^2\ 10\sigma^1$; the similarities of their equilibrium distances is clearly seen in Table 2. On the other hand, for the lowest-lying doublet state, $a\ ^2\Pi$ ($R_e = 3.812\ a_0$, $T_e = 933$ cm^{-1}), symbolized by the electronic configuration $\ldots 7\sigma^2\ 8\sigma^2\ 9\sigma^2\ 4\pi^3$ ($c_0 \approx 0.84$), the almost 8% decrease in the equilibrium distance relative to that of the ground state can be rationalized as resulting from the promotion of an electron associated with the 10σ antibonding orbital to the bonding 4π; at this distance, the configuration $\ldots 7\sigma^2\ 8\sigma^2\ 9\sigma^1\ 4\pi^3\ 10\sigma^1$ ($c_0 \approx 0.34$) also has a significant contribution. Of notice in Fig. 1, is the avoided crossing between the two $^2\Sigma^+$ states at $R \approx 3.4\ a_0$, and the ones involving the $^2\Pi$ states in the region between 4.5 and 5.2 a_0, and close to 4.2 a_0. As to the second excited $f\ ^2\Pi$ state ($T_e = 19,321$ cm^{-1}), we note that it is now mostly represented by the configuration $\ldots 7\sigma^2\ 8\sigma^2\ 9\sigma^1\ 4\pi^3$ $10\sigma^1$ ($c_0 \approx 0.82$), which results in an increased equilibrium distance ($R_e = 3.936\ a_0$), relative to the $a\ ^2\Pi$, due to the association of one electron with the antibonding 10σ orbital. For the state $g\ ^2\Pi$ ($R_e = 4.197\ a_0$, $T_e = 23,574$ cm^{-1}), the mixture of configurations $\ldots 7\sigma^2\ 8\sigma^2\ 9\sigma^2$ $4\pi^2\ 5\pi^1$ ($c_0 \approx 0.72$) and $\ldots 7\sigma^2\ 8\sigma^2\ 9\sigma^1\ 4\pi^3\ 10\sigma^1$ ($c_0 \approx 0.52$) is most significant, whereas for the state $h\ ^2\Pi$ ($R_e = 4.755\ a_0$, $T_e = 25,298$ cm^{-1}), the configurations mostly contributing are $\ldots 7\sigma^2\ 8\sigma^2\ 9\sigma^2\ 4\pi^1\ 10\sigma^2$ ($c_0 \approx 0.34$), $\ldots 7\sigma^2\ 8\sigma^2\ 9\sigma^1\ 4\pi^3\ 10\sigma^1$ ($c_0 \approx 0.41$), and

...$7\sigma^2\ 8\sigma^2\ 9\sigma^2\ 4\pi^2\ 5\pi^1$ ($c_0 \approx 0.59$). We further note that the 7σ orbital is basically the $3d_0$ orbital of arsenic. A second $^2\Sigma^-$ state dissociating into the fourth channel was also investigated and found to have a repulsive character and to lie very high in energy; at around 4.0 a_0, its energy is approximately 35,000 cm^{-1} above the ground state. We also note that to properly describe the $e\ ^2\Sigma^+$ state beyond 5.25 a_0, our state-averaged CASSCF would have to include all doublet states correlating with fifth channel, which was beyond our original plan.
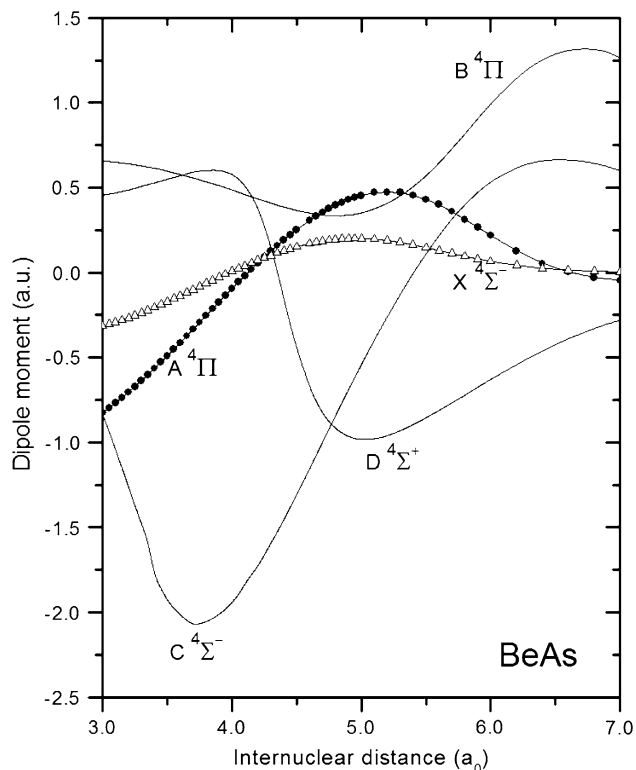

Fig. 3 The dipole moment function $\mu\ (R)$, in atomic units, for selected quartet states of the molecule BeAs

In the lack of experimental data for BeAs, to the best of our knowledge, it is worth examining how the order of states predicted for BeAs compares with those of the isovalent species BeP and BeN. The present data can be directly compared with those illustrated in Fig. 3 of Ref. [6]. A common feature is that all three molecules show two relatively low-lying excited states below about 2,550 cm^{-1}. For BeN, the $a\ ^2\Sigma^-$ ($T_e = 2,426$ cm^{-1}) and the $b\ ^2\Pi$ ($T_e = 2,532$ cm^{-1}) states are very close energetically, whereas for BeP and BeAs the energy difference between them increases significantly, with the $^2\Pi$ lower in energy. In the case of BeP, the $^2\Pi$ state lies only 502 cm^{-1} above the ground state ($X\ ^4\Sigma^-$), compared with 933 cm^{-1} for BeAs; on the other hand, the energy (T_e) of the $c\ ^2\Sigma^-$ state shifts from 1,976 cm^{-1} in BeP to 2,107 cm^{-1} in BeAs. Doublet and quartet curve crossing are likely to give rise to perturbations in the spectrum of transitions to these low-lying states. Based on the result for BeP, our first expectation was that the $^2\Pi$ state could be located below the $^4\Sigma^-$, which is not the case. As to the location of the first excited quartet states, they follow the order 9,307 cm^{-1} (BeN), 13,291 cm^{-1} (BeP), and 14,111 cm^{-1} (BeAs), and the transitions $X\ ^4\Sigma^- - A\ ^4\Pi$ would be expected to shift from the near IR part of spectrum in BeN to the red one in BeP and BeAs. Concerning the first $^2\Delta$ state, for BeP and BeAs, it is predicted to lie about 7,000 cm^{-1} above the ground state, but in BeN it was found much higher, 12,268 cm^{-1}. For all three molecules, the avoided crossing involving the two $^2\Sigma^+$ states are clearly identified in their PECs, with the one in BeP and the other in BeAs occurring in the left-hand side of the curve. Avoided crossings in BeP and BeAs are also very similar. Not described in our previous studies of BeN and BeP, this work located a very shallow PEC for the $^4\Sigma^+$ state at 35,678 cm^{-1}. As in the case of BeN and BeP, emissions from the $C\ ^4\Sigma^-$ state offer a possibility of probing the very high vibrational states of the ground state.

Table 3 Vibrational levels spacings $\Delta G_{v+1/2}$ (in cm^{-1}) for electronics states of BeAs

v	$X\ ^4\Sigma^-$	$a\ ^2\Pi$	$b\ ^2\Sigma^-$	$c\ ^2\Delta$	$d\ ^2\Sigma^+$	$A\ ^4\Pi$	$e\ ^2\Sigma^+$	$f\ ^2\Pi$	$B\ ^4\Pi$	$C\ ^4\Sigma^-$	$g\ ^2\Pi$	$h\ ^2\Pi$	$D\ ^4\Sigma^+$
0	494	661	571	524	561	545	1,045	549	500	299	434	682	327
1	492	653	558	521	556	542	935	541	482	297	466	616	292
2	488	644	545	519	549	539	895	529	472	294		568	276
3	481	635	534	516	543	535	865	516	463	292			264
4	472	624	526	512	539	529	841	500	456	289			255
5	461	613	518	507		522	818	486	449				248
6	448	602	511	500		514	796	483	442				241
7	434	593	505	493		506	774		435				235
8	420	586	498	473		498			428				229
G_0	248	334	289	264	282	274	575	278	258	150	216	359	182

Table 4 The rotational constant B_v (in cm^{-1}) for selected vibrational states of the low-lying electronic states of BeAs

v	$X\,^4\Sigma^-$	$A\,^2\Pi$	$b\,^2\Sigma^-$	$c\,^2\Delta$	$d\,^2\Sigma^+$	$A\,^4\Pi$	$e\,^2\Sigma^+$	$f\,^2\Pi$	$B\,^4\Pi$	$C\,^4\Sigma^-$	$g\,^2\Pi$	$h\,^2\Pi$	$D\,^4\Sigma^+$
0	0.4366	0.5133	0.4417	0.4412	0.4526	0.4761	0.5701	0.4799	0.4219	0.2568	0.4232	0.3324	0.4372
1	0.4330	0.5101	0.4381	0.4390	0.4488	0.4733	0.5560	0.4742	0.4252	0.2568	0.4228	0.3343	0.4175
2	0.4285	0.5064	0.4341	0.4362	0.4446	0.4698	0.5454	0.4646	0.4093	0.2566	0.4293	0.3346	0.4024
3	0.4237	0.5021	0.4301	0.4329	0.4404	0.4657	0.5375	0.4628	0.4042	0.2563			0.3895
4	0.4186	0.4972	0.4263	0.4291	0.4359	0.4613	0.5305	0.4564	0.3993	0.2557			0.3783
5	0.4132	0.4920	0.4226	0.4252		0.4568	0.5238	0.4496	0.3948	0.2547			0.3682
6	0.4072	0.4866	0.4190	0.4211		0.4518	0.5175	0.4435	0.3903				0.3588
7	0.4009	0.4810	0.4155	0.4166		0.4469	0.5111	0.4423	0.3860				0.3501
8	0.3942	0.4752	0.4193	0.4119		0.4420	0.5041		0.3817				0.3419
9	0.3873	0.4689	0.4084	0.4069		0.4372			0.3775				0.3340

A comparison of the energies at the dissociation limit also offers a way of assessing the quality of our calculations. Table 1 lists the theoretical dissociation energies of the $(\Lambda + S)$ states, and also experimental relative energies expressed as a weighted average over the corresponding multiplets using the excitation energies of Radzig and Smirnov [25]. As clearly seen in this table, our theoretical predictions are very good, differing by 225 cm^{-1}, on the average, from the experimentally derived values for the four excited dissociation channels.

Concerning the dissociation energies (D_e), listed in Table 2, the molecule BeAs in its ground state is predicted to be slightly less bound, 23.87 kcal/mol (8,348 cm^{-1}), than its isovalent partners BeP, 27.57 kcal/mol (9,643 cm^{-1}), and BeN, 31.59 kcal/mol (11,049 cm^{-1}). For the three very low-lying doublets dissociating into the second channel, the dissociation energies are 51.95 ($a\,^2\Pi$), 48.48 ($b\,^2\Sigma^-$), and 34.54 ($c\,^2\Delta$) kcal/mol, about 5–6 kcal/mol smaller than the corresponding ones in BeP. Combining the D_e values with the zero-point energies listed in Table 3, the spectroscopic dissociation energies (D_0) can be easily derived.

3.2 Vibrational energies and spectroscopic constants

In Table 3, are summarized data for the vibrational spacings, $\Delta G_{v+1/2} = G(v+1) - G(v)$, for all bound electronic states investigated in this work. These values were next used in a least-square fitting procedure with standard expressions to evaluate the vibrational constants listed in Table 2. The rotational constants B_v were evaluated as the vibrational average $\langle v|16.8578/\mu R^2|v\rangle$, where $|v\rangle$ stands for the vibrational wavefunction, and the numerical factor makes B_v directly expressed in cm^{-1}. These constants, which will permit a more direct comparison with experimental data when they become available, are collected in Table 4. Further, we stress that for a consistent comparison of theoretical constants with experimental data, it is
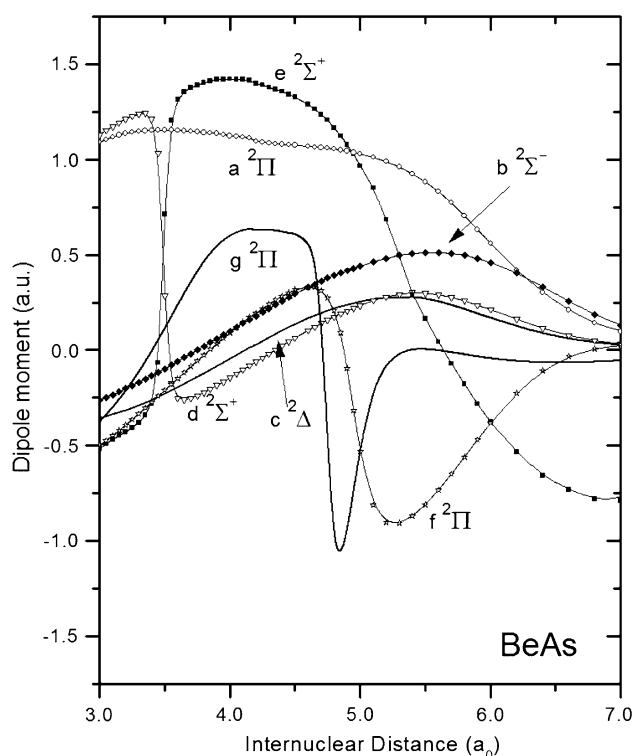

Fig. 4 The dipole moment function $\mu(R)$, in atomic units, for selected doublet states of the molecule BeAs

advisable to specify the number of points and parameters used in the fitting procedure; this is also true for the experimental constants as discussed by Richards et al. [26]. In general, the harmonic vibrational frequency is less sensitive to the number of fitting points, so it is expected to be accurate to within 1 cm^{-1} for the most favorable cases, and within a few cm^{-1} for the cases with less fitting points. The uncertainty in the equilibrium rotational constant should in the fourth decimal place. The equilibrium distances were obtained by locating the minimum in the potential energy curves and the uncertainty in their values

should be in the third decimal place. The anharmonic constants listed in Table 2 were written with three decimal digits just to reflect numerical precision. For the cases with more fitting points, they should be accurate to within 2–3 decimal places.

3.3 Dipole moment functions

Dipole moments as a function of the internuclear distance are depicted separately in Figs. 3 and 4 for selected quartet and doublet states, respectively. We note that a positive value of the dipole moment corresponds to the Be^+As^- polarity. Around the equilibrium distance, the dipole moment functions show an approximately linear behavior, and all tend to zero at large distances reflecting the neutral

Fig. 5 Potential energy curves of the ground and the lowest-lying doublet spin–orbit states (Ω) of the molecule BeAs

character of dissociating fragments. Complementing this picture, we collected in Table 4 vibrationally averaged dipole moments ($\langle\mu\rangle_v$), a quantity more directly subjected to experimental assessment. Concerning the quartets, they all have a relatively small averaged dipole moment, the largest one being that of the $B\,^4\Pi$ state of about 1.0 Debye. Therefore, in its ground electronic and vibrational states, the molecule is only very slightly polarized, $\langle\mu\rangle_0 = 0.14$ D, and the first excited $A\,^4\Pi$ state has an inverted polarity, $\langle\mu\rangle_0 = -0.31$ D. As to the doublets, for the three lowest-lying states their dipole moment functions are relatively smooth, with the $a\,^2\Pi$ state showing the largest averaged moment, $\langle\mu\rangle_0 = 2.90$ D; for the $b\,^2\Sigma^-$ state, it is an order of magnitude smaller, 0.38 D, and for the $c\,^2\Delta$ state it is even smaller, 0.004 D. For the two $^2\Sigma^+$ states, the abrupt changes close to 3.5 a_0 reflect the changes of character in the wavefunctions in the region of avoided crossing; similar changes are also observed for the higher-lying $^2\Pi$ states.

3.4 Potential energy curves for the ground and the lowest-lying doublet spin–orbit states (Ω)

Complementing the adiabatic characterization described in the previous sections, we show in Fig. 5 the potential
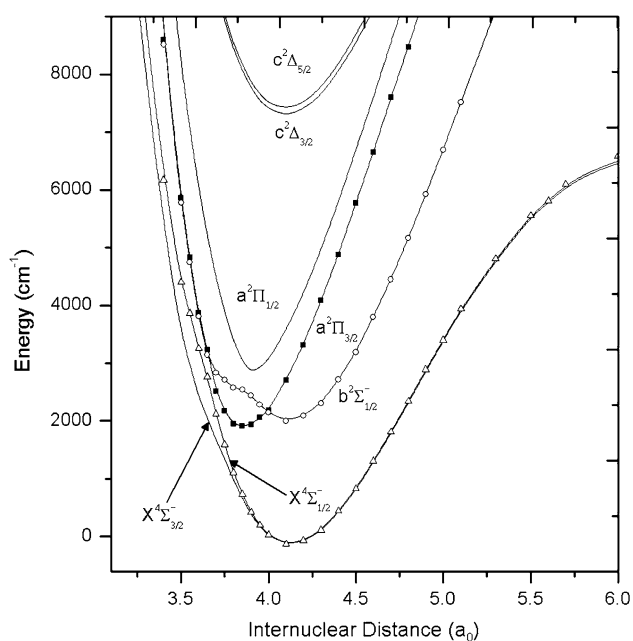
Table 6 Spectroscopic constants for the spin–orbit (Ω) states of BeAs

Ω	R_e (a_0)	T_e (cm^{-1})	G_0 (cm^{-1})	$\Delta G_{1/2}$ (cm^{-1})
$X\,^4\Sigma^-_{1/2}$	4.148	0	247	490
$X\,^4\Sigma^-_{3/2}$	4.127	10	234	465
$a\,^2\Pi_{3/2}$	3.882	1,917	389	763
$b\,^2\Sigma^-_{1/2}$	4.120	2,107	293	614
$a\,^2\Pi_{1/2}$	3.940	3,075	396	780
$c\,^2\Delta_{3/2}$	4.084	7,317	290	566
$c\,^2\Delta_{5/2}$	4.103	7,437	275	546

Table 5 Vibrationally averaged dipole moments (in Debye) for selected vibrational states of the electronic states of BeAs

v	$X\,^4\Sigma^-$	$a\,^2\Pi$	$b\,^2\Sigma^-$	$c\,^2\Delta$	$d\,^2\Sigma^+$	$A\,^4\Pi$	$e\,^2\Sigma^+$	$f\,^2\Pi$	$B\,^4\Pi$	$C\,^4\Sigma^-$	$g\,^2\Pi$	$h\,^2\Pi$	$D\,^4\Sigma^+$
0	0.1359	2.8982	0.3804	0.0038	−0.2947	−0.3059	3.3769	0.1622	1.0952	−0.0182	1.5913	−1.3416	−0.9433
1	0.1497	2.8889	0.4050	0.0198	−0.2631	−0.2927	3.5281	0.2002	1.0716	−0.0324	1.5367	−1.6334	−0.8523
2	0.1654	2.8795	0.4309	0.0386	−0.2295	−0.2275	3.7046	0.2348	1.0542	−0.0428	1.4849	−1.7336	−0.7692
3	0.1809	2.8700	0.4570	0.0593	−0.1948	−0.1821	3.7883	0.2695	1.0429	−0.0492			−0.6931
4	0.1955	2.8606	0.4818	0.0808	−0.1581	−0.1354	3.7673	0.3048	1.0362	−0.0512			−0.6246
5	0.2094	2.8514	0.5053	0.1024		−0.0883	3.7473	0.3356	1.0342	−0.0423			−0.5611
6	0.2225	2.8427	0.5279	0.1239		−0.0401	3.7812	0.3450	1.0367				−0.5019
7	0.2340	2.8345	0.5498	0.1458		−0.0054	3.8121	0.3150	1.0438				−0.4470
8	0.2424	2.8265	0.5711	0.1677		−0.0494	3.7950		1.0559				−0.3958
9	0.2504	2.8186	0.5921	0.1899		−0.0909			1.0732				−0.3481

Table 7 Percentage composition of the spin–orbit (Ω) states in terms of the ($\Lambda + S$) states of BeAs

R/a_0	$X\ ^4\Sigma^-_{1/2}$	$X\ ^4\Sigma^-_{3/2}$	$a\ ^2\Pi_{3/2}$	$b\ ^2\Sigma^-_{1/2}$	$a\ ^2\Pi_{1/2}$	$c\ ^2\Delta_{3/2}$	$c\ ^2\Delta_{5/2}$
3.5	$^4\Sigma^-$ (3) + $^2\Pi$ (97)	$^4\Sigma^-$ (3) + $^2\Pi$ (97)	$^4\Sigma^-$ (97) + $^2\Pi$ (3)	$^4\Sigma^-$ (97) + $^2\Pi$ (3)	$^2\Sigma^-$ (99)	$^2\Delta$ (100)	$^2\Delta$ (100)
3.8	$^4\Sigma^-$ (97) + $^2\Pi$ (2)	$^4\Sigma^-$ (77) + $^2\Pi$ (23)	$^4\Sigma^-$ (23) + $^2\Pi$ (77)	$^2\Sigma^-$ (6) + $^2\Pi$ (92)	$^2\Sigma^-$ (94) + $^2\Pi$ (6)	$^2\Delta$ (100)	$^2\Delta$ (100)
4.1	$^4\Sigma^-$ (98)	$^4\Sigma^-$ (98) + $^2\Pi$ (2)	$^4\Sigma^-$ (2) + $^2\Pi$ (97)	$^2\Sigma^-$ (98) + $^2\Pi$ (2)	$^2\Sigma^-$ (2) + $^2\Pi$ (98)	$^2\Delta$ (100)	$^2\Delta$ (99)
4.5	$^4\Sigma^-$ (99)	$^4\Sigma^-$ (99)	$^2\Pi$ (96) + $^2\Delta$ (3)	$^2\Sigma^-$ (100)	$^2\Sigma^-$ (1) + $^2\Pi$ (99)	$^2\Delta$ (99) + $^2\Pi$ (1)	$^2\Delta$ (86) + $^2\Pi$ (14)
6.0	$^4\Sigma^-$ (100)	$^4\Sigma^-$ (100)	$^2\Pi$ (85) + $^2\Delta$ (15)	$^2\Sigma^-$ (100)	$^2\Sigma^-$ (1) + $^2\Pi$ (99)	$^2\Delta$ (99) + $^2\Pi$ (1)	$^2\Delta$ (86) + $^2\Pi$ (14)

energy curves for the ground ($X\ ^4\Sigma^-$) and the lowest-lying doublet spin–orbit states (Ω); the former one correlates with the first dissociation channel, and the doublets with the second dissociation channel. To better appreciate the overall picture of these states, we first recall that for the corresponding ($\Lambda + S$) states, shown in Fig. 1, the $^2\Pi$ crosses both the ground and the $^2\Sigma^-$ states. Next, to obtain the symmetries of the Ω states labeled in Fig. 5, we carried out the direct product of the irreducible representation $E_{1/2}$ in the relativistic double group associated with a spin 1/2 with the irreducible representations $^2\Pi$, $^2\Sigma^-$, and $^2\Delta$. For the $^2\Pi$ state, this direct product results in two irreducible representations, $E_{1/2}$ and $E_{3/2}$, and the corresponding states are denoted $^2\Pi_{1/2}$ and $^2\Pi_{3/2}$; for the $^2\Sigma^-$ state, we have only one $\Omega = 1/2$ state ($^2\Sigma^-_{1/2}$), and for the $^2\Delta$, we obtain $^2\Delta_{3/2}$ and $^2\Delta_{5/2}$. In the case of the $^4\Sigma^-$ state, it is split into two Ω states denoted $^4\Sigma^-_{1/2}$ and $^4\Sigma^-_{3/2}$. (Table 5).

An interesting physical feature not seen in Fig. 1 for the ($\Lambda + S$) states that is now evident in Fig. 5 is an avoided crossing between the $\Omega = 1/2$ states arising from the $^2\Sigma^-$, $^2\Pi$, and $^4\Sigma^-$ states. This avoided crossing makes the first $\Omega = 1/2$ state very anharmonic. We also note that the two states 3/2 ($^2\Pi_{3/2}$) and 1/2 ($^2\Sigma^-_{1/2}$) now have quite distinct curvatures and equilibrium distances, as shown in Table 6. In the case of the Ω states arising from the $^2\Delta$ state, the energy splitting is very small, approximately 120 cm^{-1} at their equilibrium distances, with the $^2\Delta_{3/2}$ state lower in energy. Spin–orbit coupling involving the $^4\Sigma^-$ state, although very small for internuclear distances greater than approximately 3.8 a_0, becomes noticeable for shorter distances as the two $\Omega = 3/2$ states arising from the $^2\Pi$ and $^4\Sigma^-$ states avoid each other. The ground state has $^4\Sigma^-_{1/2}$ symmetry with the $^4\Sigma^-_{3/2}$ state higher by only 10 cm^{-1} at their equilibrium distances, however, due to the avoided crossing between the $\Omega = 3/2$ states this order is reversed for short distances. At the dissociation limit, the doublet states should correlate with the Be($^2S_{1/2}$) + As($^2D_{3/2}$) and Be($^2S_{1/2}$) + As($^2D_{5/2}$) channels, which are known experimentally to be apart by 320.2 cm^{-1} [25]. Since this is the only experimental data that can be of direct comparison with our results, we extended the calculation of the Ω curves up to $R = 20.0\ a_0$ and followed the dissociation of these curves. At this limit, the first two curves ($\Omega = 1/2$ and $\Omega = 3/2$) correlate with the channel Be($^2S_{1/2}$) + As($^2D_{3/2}$), whereas the other three with the channel Be($^2S_{1/2}$) + As($^2D_{5/2}$) higher in energy by 327 cm^{-1}, a result in excellent agreement with the available data. The composition of the Ω states in terms of the ($\Lambda + S$) basis as a function of the internuclear distance is summarized in Table 7 and clearly shows the changes of character of the Ω states.

4 Conclusion

This work represents the first theoretical description of the species BeAs yet unknown experimentally. It offers a high-level reliable global view of a manifold of quartet and doublet electronic states, and an accurate set of spectroscopic constants, including a description of spin–orbit effects on the lowest-lying doublet and quartet Ω states. Of course, to achieve spectroscopic accuracy further improvements like the inclusion of core-valence correlation effects, basis set extrapolation to the complete basis set limit, and further extension of the N-particle basis set, by decreasing the coefficient threshold for configuration selection, would be desirable. However, based on previous calculations for systems with about the same number of electrons, where comparisons could be made with experimental data, we are certain that the present characterization can motivate and guide, both qualitatively and quantitatively, spectroscopists in the search of this new molecule.

References

1. Machado FBC, Roberto-Neto O, Ornellas FR (1998) Chem Phys Lett 284:293
2. Valentim ARS, Ornellas FR (1994) J Phys Chem 98:12570
3. Borin AC, Ornellas FR (1993) J Chem Phys 98:8761
4. Ornellas FR, Roberto-Neto O, Borin AC, Machado FBC (1991) J Chem Phys 95:9086
5. Machado FBC, Ornellas FR (1989) Mol Phys 67:1129

6. Ornellas FR (2009) J Phys B At Mol Opt Phys 42:185102
7. Machado FBC, Ornellas FR (1991) J Chem Phys 94:7237
8. Borin AC, Ornellas FR (1994) Chem Phys 184:59
9. Ornellas FR, Machado FBC, Roberto-Neto O (1992) Mol Phys 77:1169
10. Herzberg G (1950) Molecular spectra and molecular structure, vol I. Spectra of diatomic molecules. Van Nostrand Reinhold, New York
11. Knowles PJ, Werner H-J (1985) J Chem Phys 82:5053
12. Werner H–J, Knowles PJ (1985) Chem Phys Lett 115:259
13. Knowles PJ, Werner H–J (1988) Chem Phys Lett 145:514
14. Werner H-J, Knowles PJ (1988) J Chem Phys 89:5803
15. Werner H–J et al (2006) Molpro-2006.1
16. Peterson KA, Figgen D, Goll E, Stoll H, Dolg M (2003) J Chem Phys 119:11113
17. Zemke WT, Stwalley WC (1981) QCPE Bull 4:79
18. Langhoff SR, Davidson ER (1974) Int J Quantum Chem 8:61
19. Rawlings DC, Davidson ER, Gouterman M (1984) Int J Quantum Chem 26:251
20. Borin AC, Ornellas FR (1999) Chem Phys 247:351
21. Ornellas FR (2006) J Chem Phys 125:114314
22. Machado FBC, Resende SM, Ornellas FR (2002) Mol Phys 100:699
23. Ornellas FR, Andreazza CM, de Almeida AA (2000) Astrophys J 538:675
24. Berning A, Schweizer M, Werner H-J, Knowles P, Palmieri P (2000) Mol Phys 98:1823
25. Radzig AA, Smirnov BM (1985) Reference data on atoms, molecule, and ions. Springer, Berlin
26. Richards WG, Raftery J, Hinkley RK (1973) In: Dixon RN (ed) Theoretical chemistry, chap 1, vol 1. The Chemical Society, London